Secondary production at the Polar Front, Barents Sea, August 2007

Sünnje L. Basedow [a,*], Meng Zhou [b], Kurt S. Tande [a]

[a] Faculty of Biosciences and Aquaculture, University of Nordland, N-8049 Bodø, Norway
[b] Department of Environment, Earth and Ocean Science, University of Massachusetts, 100 Morrissey Blvd, Boston, MA 02125, USA

A B S T R A C T

To investigate spatial patterns of secondary production we sampled four core hydrographical regions of the Polar Front in the Barents Sea (Arctic Water, ArW; Polar Front Water, PFW; Atlantic Water, AtW; and Melt Water, MW) by towing an undulating instrument platform along a transect crossing the front from August 8–9, 2007. Sensors mounted on the platform provided data on the hydrography (CTD), fluorescence (Fluorometer, F) and zooplankton abundance in the size range between 0.1 and 30 mm (Laser Optical Plankton Counter, LOPC). These continuous, biophysical data with high-spatial resolution were supplemented by discrete water and zooplankton net samples at stations for sensor calibrations. After in depth quality assessments of the biophysical data, estimates were made of the vital rates based on biovolume spectrum theory. Five size groups were distinguished from the LOPC data: small (S), mainly *Oithona* spp. and the appendicularian *Fritillaria* sp.; medium (M), mainly *Pseudocalanus* spp. and *Calanus* spp. CI–CIII; large (L), mainly *Calanus* spp. CIV–CV; and extra large (XL and 2XL), juvenile and adult euphausids. Size groups were further divided based on transparency of organisms. Vital rates based on the biophysical in situ data in combination with biovolume spectrum theories agreed generally well with data from empirical and numerical models in the literature. ArW was characterised by subsurface maxima of chlorophyll *a* (chl *a*), and an estimated population growth of ca. 13 mg C m^{-3} d^{-1} for CI–CIII *Calanus* spp. and some older *Pseudocalanus* within the chl *a* maxima. Frontal waters were characterised by low chl *a* concentrations, but high abundances and production (around 1 g C m^{-3} d^{-1}) of small copepods (*Oithona* spp.) and appendicularians (*Fritillaria* sp.). The estimated production of small-size zooplankton was an order of magnitude higher than the production of all other size groups combined, including large copepods. The high loss rates (-166 to -271 mg C m^{-3} d^{-1}) of small zooplankton may contribute a substantial amount of carbon to the benthos and to pelagic predators such as young capelin. AtW was the most productive water mass, with surface chl *a* maxima and an estimated population growth of 134 mg C m^{-3} d^{-1} for small zooplankton, 3.6 mg C m^{-3} d^{-1} for medium-sized copepods and 0.9 mg C m^{-3} d^{-1} for CIV–CVI *Calanus*. For those *Calanus* spp. in the surface layer, the estimated specific mortality rates were up to -0.35 d^{-1}, partly due to high predation pressure by hydrozoans and chaetognaths.

© 2013 The Authors. Published by Elsevier B.V. Open access under CC BY-NC-ND license.

1. Introduction

Secondary production in the pelagic zone, i.e. the increase in biomass of zooplankton over a period of time, constitutes the base for the largest fisheries in the world. It has therefore been a priority research question for biological oceanographers since the onset of marine research. Despite the major interest, spatio-temporal patterns of secondary production remain largely unresolved, due to a lack of adequate methods to estimate secondary production.

Among the approaches that have been tried for estimating secondary production in marine systems are the ecological method, the cohort

method, the physiological method, the egg production method, empirical models and more recently biochemical methods (see also Poulet et al., 1995; Runge and Roff, 2000). The ecological method is based on the trophodynamic concept (Lindemann, 1942), where the production of any trophic level is estimated based on primary production and transfer efficiencies between trophic levels (Lalli and Parsons, 1997). The cohort method has been very much in use in those situations where age or stage information of a population can be analysed with a minimum degree of uncertainty (Aksnes and Magnesen, 1988; Kimmerer, 1987; Kimmerer and McKinnon, 1987). Some decades ago the physiological method was extensively explored in experimental systems, using the energy budget of an individual to calculate growth and secondary production by taking into account all input to and output from the individual (Ikeda and Motoda, 1978; Le Borgne, 1982). In response to the high degree of uncertainty in many earlier methods (Miller, 2004), the egg production method was proposed as a means to obtain globally comparable production estimates by a simplified method (Poulet et al., 1995). Production estimates are limited to female copepods, allowing for

relatively high resolution on large spatial scales (e.g. Jonasdottir et al., 2005; Stenevik et al., 2007).

In the 1990s and early 2000s, several empirical models aggregating research on vital rates of the preceding decades were introduced to provide global analyses of growth and mortality based on locomotion of animals, food availability and energy balance (Hirst and Bunker, 2003; Hirst and Lampitt, 1998; Huntley and Boyd, 1984; Huntley and Lopez, 1992). The latest empirical analysis of a large data set revealed that growth in juvenile copepods is strongly temperature-dependent, and that juveniles reach half-saturation of growth at food concentrations an order of magnitude lower than adults (Hirst and Bunker, 2003). This globally confirmed earlier findings that juveniles in nature are growing much closer to food saturation than adults (Vidal, 1980).

More recently, biochemical methods have been developed that can provide production estimates for the whole zooplankton community, not only copepods. These methods use the rate of nucleic acids (RNA/DNA), enzyme activity (specific aminoacyl-tRNA-synthetases, spAARS), or a combination of both to estimate overall metabolic activity and then growth and production (e.g. Yebra and Hernández-León, 2004). Biochemical methods might become more widely used in the future for obtaining reliable production estimates of mesozooplankton. However, spatial resolutions of any method that involves net tow sampling at stations are too low to resolve the spatial variability of mesozooplankton population processes.

Also, the knowledge on mortality rates in marine systems is limited because of the difficulties in measuring these rates (Ohman, 2012, and references therein). Most commonly vertical or horizontal life tables have been applied, which assume either a stable age-structure of a population, or repeated sampling of the same population (Aksnes and Ohman, 1996; Aksnes et al., 1997). Though many problems in relation to estimating mortality rates of a population at a particular location can be minimised by optimal sampling design (Ohman, 2012), observing spatio-temporal patterns of mortality rates remains a challenge. To our knowledge, the only global approximation of natural rates of mortality has been provided by Hirst and Kiørboe (2002). Their empirical analysis of field data predicts that mortality rate in copepods increases with temperature and declines with body weight. Furthermore, the analysis reveals that small copepods seem to be able to avoid some agent of mortality that other similar-sized pelagic animals do not (Hirst and Kiørboe, 2002).

These previous studies have contributed to a valuable synthesis of empirical information on vital rates in copepods and have provided new understanding on the underlying patterns with regard to growth and mortality. We may have reached a stage where we have extracted what is possible from a clearly under-sampled system, and where further progress will come only after using new approaches that allow for high-resolution sampling (Bi et al., 2011; Hirst and Bunker, 2003). The present study uses the latest models based on biovolume spectrum theories to estimate vital rates in a spatially heterogeneous area, and is thus a response to the repeated call for improved methods to measure spatial patterns of growth, mortality and production of marine zooplankton (e.g. Hirst and Bunker, 2003; Miller, 2004; Ohman, 2012; Plourde et al., 2009; Skarðhamar et al., 2011).

Biovolume spectrum theories are ecological theories tailored to optical instruments that observe plankton distribution in size classes. They were developed as an alternative approach to the classical modelling of the marine food web when it was realised that plankton biomass is distributed systematically along size classes, and that energy fluxes through the spectrum can be described by size-dependent physiological and vital rates (Platt and Denman, 1978; Sheldon et al., 1972; Silvert and Platt, 1978). In the early mathematical formulations by Platt and Denman (1978) and Silvert and Platt (1978), the flow of energy was restricted from small to larger size classes. Zhou and Huntley (1997) developed a general mathematical approach, which includes all sinks and sources contributing to the energy flow through the spectrum, and described energy fluxes based on the distribution function of

abundance and the law of the conservation of mass (see also Basedow et al., 2010b). Later, Zhou et al. (2010) refined the equations describing growth to avoid an overestimation of growth at high food concentrations and temperature, and developed a mortality model based on assimilation efficiencies and the slope of the biovolume spectrum. Applications of biovolume spectrum theories to field data are scarce, but have yielded realistic estimates of trophic levels (Basedow et al., 2010b; Tarling et al., 2012), and of growth and mortality rates of zooplankton in an enclosed fjord (Edvardsen et al., 2002). The later growth and mortality models by Zhou et al. (2010) have not been applied to field data to date.

The present study has been outlined to cover three core hydrographical regions of the Polar Front in the Barents Sea, where high spatial variability in vital rates has been predicted by biophysical models (Skarðhamar et al., 2011). For adequate resolution in sampling, this study rests on high resolution data obtained by new technology platforms (see Basedow et al., 2010b) which, after in depth quality assessments, are followed by estimates of vital rates in the zooplankton community based on biovolume spectrum theories (Zhou et al., 2010). The combined use of conductivity–temperature–depth–fluorescence sensors (CTD-F) and laser optical plankton counter (LOPC) has been proven to be a powerful tool in generating environmental and plankton data with high spatial resolutions based on semi-automatic sampling. The quantitative nature of the LOPC has been further ascertained by an intercalibration study of video plankton recorder and LOPC (Basedow et al., 2013).

The objectives are (i) to compare rates estimated based on biovolume spectrum theories with literature values, (ii) to present spatial patterns of vital rates along a transect crossing the front, and (iii) to provide growth, mortality and production rates for the mesozooplankton community within the main hydrographical regimes at the Polar Front: Atlantic Water, Arctic Water, Polar Front Water and Melt Water.

2. Methods

2.1. Study area

The Barents Sea is a highly productive Arctic shelf sea with marked differences between the Atlantic influenced areas in the south and the Arctic influenced areas in the north (Loeng, 1991). The ecosystem is fuelled by an annual gross primary production of about 120 g C m^{-2} in Atlantic influenced areas, and ca. 60 g C m^{-2} in seasonally ice-covered areas according to a recent modelling study (Reigstad et al., 2011). The topography of the Barents Sea includes many deep channels (>300 m) and shallow banks. An inflow of Atlantic water from the Norwegian Sea brings in heat and salt and during spring and summer, zooplankton biomass (Edvardsen et al., 2003). The influx of zooplankton is largely controlled by climatic forcing, but when it enters the Barents Sea the zooplankton are utilised mainly by planktivorous fish, which can exert strong predation pressure masking the effect of climatic forcing (Stige et al., 2009). The biomass of higher trophic levels, e.g. capelin (*Mallotus villosus*), cod (*Gadus morhua*) and herring (*Clupea harengus*), in the Barents Sea is an order of magnitude higher than in comparable subarctic ecosystems that lack the influx of zooplankton (Hunt et al., 2013).

The Polar Front in the Barents Sea separates warmer, more saline Atlantic Water (AtW) from colder, less saline Arctic Water (ArW) (Loeng, 1991). It is tightly coupled to topography in the western part, while less so in the eastern part of the Barents Sea where the position of the front is more variable.

2.2. Field sampling

Data presented here stem from an area of the Polar Front in the west, close to Storbanken, which was visited during a cruise with R/V "Jan Mayen" as part of the International Polar Year project NESSAR in August 2007 (Fig. 1). The NESSAR project focused on biophysical interactions at frontal systems in the Norwegian and Barents Sea. During two crossings

of the Polar Front, physical-biological data were collected in the surface layer (2–75 m) by an undulating instrument platform (Scanfish; GMI, Denmark) that was towed at 7 knots along two ca. 120 km long transects (Fig. 1). The sensors mounted on the platform provided physical and biological data at a rate of 2 Hz including hydrography (CTD; SBE 911plus, Seabird Electronics Inc., USA), fluorescence (F; Seapoint Chlorophyll Fluorometer, Seapoint Sensors Inc., USA) and zooplankton abundance in the size range between 0.1 and 30 mm (Laser Optical Plankton Counter, LOPC; Brooke Ocean Technology Ltd., Canada). The continuous tows with the LOPC-CTD-F instrument package were conducted from August 8 to 9. After the tows, discrete water (5 L Niskin bottles) and zooplankton net samples (Multinet, 180 μm mesh width, 0.25 m² mouth opening, Hydrobios, Kiel, Germany) were taken at 5 stations during August 9–13. From the discrete water samples, three replicates of 250 mL each were filtered through GF/C filters, which were then wrapped in aluminium and frozen for analysis of chlorophyll a (chl a) ashore. We calibrated the fluorescence sensor of the Scanfish against filtrated chl a by flushing the remaining water of the Niskin bottles through the sensor, and fitted a regression equation to chl a vs. fluorescence as described in Basedow et al. (2006). Five depth layers were sampled by the Multinet during vertical hauls. These layers were selected based on CTD-F profiles taken prior to the Multinet sampling. Zooplankton samples were preserved immediately in a solution of 20%

fixation agent (50% formaldehyde buffered with hexamine, 50% 1,2 propandiol) in seawater.

2.3. Analysis of water and net samples

Chl a was analysed from the frozen filters using a Turner Designs fluorometer and methanol as extractant (Holm-Hansen and Riemann, 1978). The calibration of the fluorescence sensor yielded a regression equation of

$$chl\,a = 1.243 * F - 0.0902 \tag{1}$$

with F being the fluorescence, chl a in mg m^{-3}, and the variance accounted for $r^2 = 0.84$.

The taxonomic composition of zooplankton net samples was analysed under a stereo-microscope. Species and developmental stages were identified where feasible, else the lowest feasible taxonomic level was assigned. The sibling species Calanus finmarchicus and C. glacialis were separated based on their size (Daase and Eiane, 2007). Prior to analysis, samples were split into sub-samples using a Motoda plankton splitter; from the sub-samples at least 100 individuals of Calanus spp. and other dominant species were counted. Abundances were calculated based on filtered water volumes obtained from the flowmeters of the Multinet.

2.4. Analysis and quality control of LOPC data

2.4.1. Particles counted

The laser optical plankton counter (LOPC) is an optical instrument designed to count and measure particles in the water column (Herman et al., 2004). The instrument is towed through the water, whereby zooplankton and other particles pass through a channel and their number, size and transparency are registered on a matrix of photo diodes. Two types of particles are distinguished: particles occluding one or two diodes (single element particles, SEPs), and particles occluding three or more diodes (multi element particles, MEPs). We computed the size of particles as equivalent spherical diameter (ESD) as described in the manual (Anonymous, 2006), and in more detail in Checkley et al. (2008) and Gaardsted et al. (2010). For either a SEP or MEP its size is computed by the light level relative to the background and time of its passage through the laser beam, this is termed digital size (DS). The light level relative to the background also represents an index of the transparency of a particle.

2.4.2. Transparency of particles

The LOPC not only counts zooplankton particles but also other particles such as detritus and phytoplankton colonies. Checkley et al. (2008) proposed to distinguish copepods and non-copepod particles based on their transparency. To analyse the transparency of particles they computed an attenuation index (AI), given as the ratio between mean DS of all diodes that are occluded by a MEP, and the maximum DS a diode can have. Basedow et al. (2013) used a slightly different AI, excluding the first and last diodes that are occluded by a MEP when computing mean DS. This ensures that the areas of all diodes that influence the mean DS are completely covered by the particle, which might not be the case for diodes at the edges of a particle. Including the first and last diodes might therefore lead to an artificial low AI that is not due to high transparency of a particle but due to low areal coverage of the diodes. The applicability of the AI to infer the type of particles observed may be limited (Basedow et al., 2013). Also the transparency of copepods can range from quite translucent to relatively opaque. In the study by Basedow et al. (2013), a better agreement between abundance estimates from a Video Plankton Recorder and a LOPC was obtained when those particles with a low AI were included in the abundance estimates from the LOPC. The evidence is not conclusive at present, therefore to provide further values of AIs from copepod and non-copepod
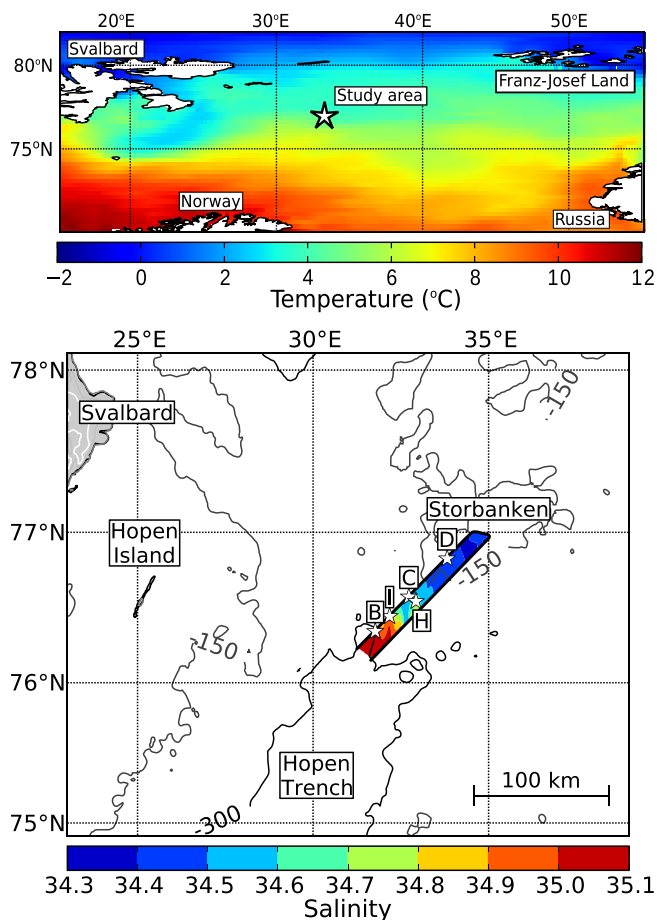

Fig. 1. Study area at the Polar Front, Barents Sea, August 2007. Top: Barents Sea. The false colours represent the sea surface temperature (SST) as observed by MODIS AQUA on August 12, 2007 (Rutledge et al., 2006). The star depicts the approximate location of the study area. Bottom: The bathymetry of the study area indicated by the star in the top panel. The 2 solid black lines indicate the 2 transects along which the Scanfish–CTD–F-LOPC was towed. The white stars indicate locations where vertical net hauls with a Multinet were performed. The false colours represent salinity at 20 m observed by the CTD mounted on the Scanfish. Bottom topography is produced from the ETOPO1 data set (Amante and Eakins, 2009).

dominated communities, we computed the AI as described in Basedow et al. (2013).

2.4.3. Faulty data

In turbid waters off the Brazilian coast, Schultes and Lopes (2009) detected faulty registrations of MEPs in their data. The MEP signal in the data file was observed to be incoherent, i.e. the information on the diodes occluded by a MEP was arranged disorderly (see Schultes and Lopes (2009) for an example of an incoherent MEP). Possibly the LOPC was sensing coloured dissolved organic matter, which led to an overload of the MEP signal despite abundances of zooplankton being far below the upper limit of the LOPC of 10^6 particles m^{-3} (Schultes and Lopes, 2009). To rapidly detect sampling stations with artificial high numbers of MEPs, Schultes and Lopes (2009) proposed to compute the ratio between total counts (TC) and MEPs, and to view stations with a TC/MEP ratio less than 20 with caution. We followed their example and computed the TC/MEP ratio for each of our 14 data files. TC/MEP ratios less than 20 (17 and 19, respectively) were observed in the two data files on the Arctic side of the front, but no faulty registrations of MEPs were detected in these files. We did, however, observe faulty data in the 4 data files that were located in the centre of the transect. In these 4 data files the TC/MEP ratios were not less than 20, but 832 out of 823,550 MEPs, i.e. 0.1% of the MEPs from that area, were considered faulty. Because of their low numbers, we chose not to exclude the data in those files from further analyses, but these data from the central part of the transects have to be viewed with some caution. No faulty registrations of MEPs were detected in ArW or AtW.

2.4.4. Size classification

Particles counted by the LOPC were separated into 5 size groups, and main zooplankton species/groups within each size group were determined based on literature values (Basedow et al., 2006, 2010a,b; Beaulieu et al., 1999; Edvardsen et al., 2002; Gaardsted et al., 2010; Herman and Harvey, 2006) and on the abundances of species in the Multinet samples from our study area (Tables 2, 3). The smallest size group (S) was very diverse containing omnivore copepods (Oithona, Microcalanus, Triconia), Calanus nauplii, hydrozoans, mesopelagic invertebrate larvae, and appendicularians (cf. Basedow et al., 2010a; Beaulieu et al., 1999). Of the appendicularians, living Oikopleura with houses are registered somewhere between3 and 10 mm ESD, depending on the clogging (cf. Basedow et al., 2010a; Beaulieu et al., 1999). However, the majority of the appendicularians observed in this study, belonged to the smaller Fritillaria (Table 2). Based on the distribution patterns of transparent particles at the front, and on the net samples, it is very likely that Fritillaria, and thus the majority of appendicularians, were registered in the S size class. When towing the LOPC at 7 knots, as in this study, fragile particles are likely to be destroyed due to turbulent flow at the aperture of the instrument (Edvardsen et al., 2002). Discarded houses of appendicularians are fragile, and were likely fragmented into particles smaller than 0.3 mm ESD, and therefore counted either as particles belonging to the S size group or as even smaller particles, which we excluded from our analyses.

Herbivore and omnivore copepods were the most important species in the medium size group (M), but it also included more transparent hydrozoans and chaetognaths. Chaetognaths had a size of 5.98 ± 3.61 mm (mean ± SD, n = 99), corresponding to an ESD of 0.5–1.9 mm (cf. Basedow et al., 2010a; Beaulieu et al., 1999). The large size group (L), transparent and more opaque plankton, contained Calanus CIVs and CVs, the few larger chaetognaths and possibly also larger hydrozoans (cf. Basedow et al., 2010a; Beaulieu et al., 1999). Though only relatively low numbers of Calanus CIV and CV were observed in the Multinet samples, it is highly likely that the majority of the more opaque animals in the large size group were Calanus CIV and CV. At higher latitudes, krill larvae are the only other mesozooplankton numerically important that has the same size and transparency signature as older stages of Calanus spp. (Basedow et al., 2010a; Edvardsen et al., 2002). No krill larvae were observed in the Multinet samples, while juvenile and adult krill were observed in live samples from a macrozooplankton trawl that was operated along the transect during the time of the study. However, their distribution pattern did not match the distribution pattern of the large, more opaque size group observed by the LOPC (C. Broms, Institute of Marine Research, unpublished data). Furthermore, the adult Meganyctiphanes norvegica and Thysanoessa inermis that were observed in AtW in the macrozooplankton trawl samples are too large to be registered by the LOPC. Little is known on the size signature of larger mesozooplankton registered by the LOPC, but juvenile and adult euphausids are registered somewhere between2 and 10 mm ESD (Edvardsen et al., 2002). Additional sampling with a WP2 net was carried out along the transect at 78.98 °N in ArW, which yielded abundant older stages of Calanus from 30 to 80 m, but none in the upper 30 m. This fits very well to the distribution observed by the LOPC (Fig. 3). Because of the low number of Multinet stations (five) and the patchy distribution of zooplankton, it is therefore likely that the Multinet sampling missed the patches of older stages of Calanus spp. that were observed by the LOPC.

Abundance estimates of particles across the Polar Front with two different sizes and transparencies are shown in Fig. 3. The small- to medium-sized (0.5–1 mm ESD), transparent (AI < 0.4) particles consisted of hydrozoans, chaetognaths, and likely mostly of appendicularians, while the small-medium sized, more opaque particles were mainly represented by small, omnivore copepods, Pseudocalanus and CI–CIII copepodites of Calanus. The larger (1–2 mm ESD), transparent group (AI < 0.4) was made up by chaetognaths and likely hydrozoans, and the larger, more opaque (AI > 0.4) group by older developmental stages of Calanus spp. (ref. Table 3).

2.5. Biovolume spectra

Biovolume spectra are the analogue to biomass spectra, and their shape is defined by energy fluxes within pelagic systems (e.g. Platt and Denman, 1978; Zhou, 2006; Zhou and Huntley, 1997). The intercept of the biovolume spectrum indicates the productivity of a system, with more productive systems being represented by spectra with higher intercepts. Energy recycling within a system determines the slope of the biovolume spectrum, hence the slope can indicate the trophic state of a system (Basedow et al., 2010b; Zhou, 2006). Developing mesozooplankton cohorts can often be identified in a biovolume spectrum as waves propagating along the spectrum (Silvert and Platt, 1978; Zhou and Huntley, 1997). We computed the normalised biovolume spectrum b, as defined by

$$b = \frac{\text{biovolume in size interval } \Delta w}{\text{size interval } \Delta w} \left(\text{in m}^{-3} \right) \qquad (2)$$

for the different water masses. Based on the spectra and on computed growth, we estimated mortality and production in the mesozooplankton community as described below.

Table 1
Multinet stations. Sampling locations and times (August 2007) of 5 stations along a transect crossing the Polar Front in the Barents Sea. The first net of the Multinet was opened ca. 20 m above the bottom.

Station	Location	Date	UTC	Lon (°E)	Lat (°N)	Sampling intervals
B	Atlantic	09 Aug	09:09	31.77	76.35	270–150–75–50–25–0
C	Deep front	10 Aug	14:50	32.73	76.58	225–120–75–50–25–0
D	Arctic	11 Aug	09:57	33.82	76.83	100–75–50–25–0
H	Deep front	12 Aug	10:16	32.93	76.55	180–100–75–50–25–0
I	Shallow front	13 Aug	07:37	32.18	76.45	240–150–75–50–25–0

Table 2
Composition of the mesozooplankton community at the Polar Front around Storbanken in August 2007. Abundances are given as individuals m^{-3}. Three sampling layers are shown for the 5 stations, the lower layer is averaged from the three lower nets of the Multinet. For the location of stations see Fig. 1 and Table 1.

Species/group	B — Atlantic			I — Shallow front			H — Deep front			C — Deep front			D — Arctic		
	270–50	50–25	25–0	240–50	50–25	25–0	180–75	50–25	25–0	225–50	50–25	25–0	100–50	50–25	25–0
Calanus spp. nauplii	–	–	0.9	1.0	0.7	13.3	7.3	13.0	43.1	3.7	8.0	108.8	9.3	38.0	60.0
C. finmarchicus CI–CIII	4.6	29.3	4.9	9.5	4.7	13.0	13.3	36.3	44.9	9.6	14.4	23.2	24.7	77.0	57.0
C. finmarchicus CIV–CV	23.4	–	1.8	21.9	1.7	0.3	45.3	6.5	4.3	42.5	15.6	10.8	1.9	1.0	0.8
C. glacialis CI–CIII	0.9	7.1	0.7	1.6	–	1.0	15.0	11.5	30.8	3.3	0.8	4.4	23.7	29.0	77.0
C. glacialis CIV–CV	4.4	–	0.9	2.6	–	–	16.7	1.5	0.6	11.1	–	0.4	1.9	1.4	1.8
C. hyperboreus CI–CIII	–	–	0.4	–	–	–	–	0.3	–	–	–	1.2	–	–	–
C. hyperboreus CIV–CV	1.4	–	0.2	0.1	–	–	–	–	–	0.4	–	–	–	–	–
Metridia spp. CI–CV	24.1	7.8	1.1	35.8	3.0	1.3	133.1	8.5	3.2	128.0	2.8	2.8	4.7	3.2	1.0
Metridia spp. adult	2.0	–	–	–	–	–	1.3	–	–	3.4	–	–	–	–	–
Pseudocalanus spp. CI–CV	10.7	172.8	6.2	26.5	16.0	53.3	27.9	251.0	369.2	31.3	254.0	345.6	69.5	528.0	384.0
Pseudocalanus spp. adult	1.1	25.6	0.4	2.2	0.3	3.3	3.8	7.0	1.5	1.6	2.0	19.2	1.5	–	–
Microcalanus spp.	31.8	326.4	2.7	111.1	28.7	23.3	46.1	4.0	–	67.0	6.0	12.8	9.2	6.0	–
Oithona similis CI–CV	22.5	236.8	252.0	62.3	115.3	813.3	48.9	225.0	520.0	113.0	416.0	627.2	138.7	446.0	542.0
Oithona similis adult	22.1	275.2	42.0	92.9	165.3	246.7	49.7	37.0	440.0	68.3	72.0	332.8	88.1	114.0	148.0
Oithona spinirostris	–	–	–	11.6	2.0	3.3	2.9	–	–	–	–	–	1.4	–	–
Triconia borealis	2.3	0.7	4.9	4.5	4.0	–	6.2	4.0	3.1	8.4	28.0	70.4	4.0	2.0	8.0
Cladocera	–	–	0.5	0.4	1.3	33.3	–	–	1.5	–	–	–	–	–	–
Hydrozoa	1.6	5.0	150.7	2.3	1.0	516.7	–	0.3	2.2	1.6	–	12.8	0.1	–	–
Ctenophora larvae	–	–	–	1.6	8.0	16.7	–	–	3.1	–	–	–	–	–	–
Echinodermata larvae	8.9	37.7	13.1	14.4	19.3	30.0	3.2	35.0	9.2	25.1	72.0	32.0	4.1	54.0	4.0
Chaetognatha indet.	–	–	–	–	0.7	3.3	–	1.0	0.6	–	–	12.8	0.4	0.6	2.0
Parasagitta elegans	1.1	7.1	56.9	1.2	1.3	–	0.5	0.5	2.6	3.1	1.2	–	0.3	–	–
Limacina helicina juveniles	–	–	–	1.6	3.3	10.0	2.5	2.0	18.5	–	–	–	4.1	46.0	40.0
Gastropoda juveniles	0.2	–	3.3	–	–	–	–	–	–	5.3	12.8	32.0	–	–	–
Bivalvia juveniles	4.1	12.1	8.0	14.8	18.7	76.7	1.9	8.0	64.6	7.5	46.0	51.2	2.2	2.0	2.0
Polychaeta larvae	0.1	–	–	1.6	4.7	13.3	1.1	16.0	3.1	0.1	–	–	1.8	2.0	14.0
Fritillaria borealis	0.1	0.7	1.1	6.1	7.3	120.0	2.4	143.0	227.7	125.7	96.0	409.6	7.4	20.0	30.0
Oikopleura spp.	10.6	5.7	0.4	22.3	18.0	46.7	28.5	39.0	70.1	98.5	66.0	185.6	2.3	34.0	50.0

2.6. Estimating growth and production

Growth was computed based on the observed data on temperature, chl *a* and zooplankton in three steps: (1) binning zooplankton counts into 56 size bins that were equally spaced on a logarithmic scale, (2) computing weight *w* (in mg C individual^{-1}) for each size bin by converting biovolume to carbon and (3) computing weight-specific growth *g* (in day^{-1}) for each size bin according to Zhou et al. (2010) and Hirst and Bunker (2003), see below. Production *P* (normalised by size bin) is then given as

$$P = g * w * N / \mathrm{d}w \left(\text{in mg C m}^{-3} \text{ d}^{-1} \right) \tag{3}$$

where *N* is the abundance in individuals m^{-3}. Two different methods to estimate growth were compared: first the purely empirical estimates by Hirst and Bunker (2003), and secondly the

combined theoretical–empirical estimates by Zhou et al. (2010). Using Hirst and Bunker (2003) (their Table 6) weight-specific growth (*g*, day^{-1}) is given as

$$g(w, T, C_a) = 10^{aT} w^b C_a^c 10^d \tag{4}$$

where *w* is the body weight in μg carbon individual^{-1}, *T* the temperature in °C, C_a the food concentration in mg chl *a* m^{-3}, and a, b, c and d are constants equal to 0.0186, −0.288, 0.417 and −1.209, respectively (Hirst and Bunker, 2003). Zhou et al. (2010) derived a semi-empirical equation to estimate growth by combining the empirical equations of Hirst and Bunker (2003) with the theoretical definitions of growth by Huntley and Boyd (1984) and with theoretical and empirical considerations in relation to clearance rate. Weight-specific growth is then defined as

$$g(w, T, C_a) = 0.033 \left[C_a / \left(C_a + 205 e^{-0.125T} \right) \right] e^{0.09T} w^{-0.06} \tag{5}$$

where *w* is in mg C individual^{-1} and C_a in mg carbon m^{-3} (Zhou et al., 2010, their Eq. 19). For both methods, i.e. Hirst and Bunker (2003) and Zhou et al. (2010), body volume of the particles was converted into carbon using a ratio of mg carbon = 0.0475 body volume (Gallienne et al., 2001). For the method of Zhou et al. (2010) chl *a* was converted to carbon (C) using a ratio of C:chl *a* = 50, which is a ratio commonly observed (e.g. Reigstad et al., 2008). The sensitivity of modelled growth estimates to the conversion ratios was tested by applying a range of other ratios: for C:body volume these were 0.02375, 0.04275, 0.05225 and 0.07125 (corresponding to a change of −50%, −10%, +10% and +50% of the original conversion factor), and for C:chl *a* the ratios tested were 25, 75 and 100 (Table 5). The comparison of the methods by Hirst and Bunker (2003) and Zhou et al. (2010) was restricted to older stages of *Calanus* spp. (large, more opaque particles), because this group is the most homogeneous functional group identified by the LOPC.

Table 3
Size classification applied to data collected by a LOPC at the Polar Front, Barents Sea in August 2007. Main species within each size class were determined based on their size signature (from literature values) and their occurrence in Multinet samples from the same area. The question marks denote that the sizes registered by the LOPC for the organisms are not known, or that organisms were not captured by the net because they were too fragile and/or too large.

Size class	ESD (mm)	Main zooplankton species
S	0.25–0.6	*Oithona* sp., *Microcalanus* spp., *Triconia* sp., *Calanus* spp. nauplii, Hydrozoa, meroplanktic larvae, Appendicularia
M	0.6–1.0	*Pseudocalanus* spp., *Calanus* spp. CI–CIII, *Metridia* sp. CI–CV, Hydrozoa, Chaetognaths
L	1.0–2.0	*Calanus* spp. CIV–CVI, Chaetognaths, Hydrozoa (?),
XL	2.0–4.0	Juvenile and adult euphausids (?)
2XL	4.0–10.0	Adult euphausids (?)

Table 4

Production, loss and population change rates. Average within water mass for each size group, in mg C m^{-3} d^{-1}. See Table 3 for species composition within size group. Based on data collected by a laser optical plankton counter at the Polar Front, Barents Sea, in August 2007. AtW = Atlantic Water, PFW = Polar Front Water, MW = Melt Water, ArW = Arctic Water.

	AtW	PFW	MW	ArW
Production				
S	1388.5	973.8	1084.3	76.1
M	94.2	41.9	27.0	16.6
L	23.4	11.5	3.2	4.3
XL	5.8	0.6	0.1	0.2
2XL	3.1	0.2	0.1	0.1
Loss				
S	−280.2	−165.8	−270.6	−14.0
M	−33.7	−21.4	−16.8	−0.1
L	−29.1	−29.8	−15.2	−5.3
XL	−6.9	−7.0	−4.8	−2.7
2XL	−22.7	−3.7	−0.3	−0.1
Population change				
S	133.6	135.1	−26.1	19.1
M	3.6	−5.3	−5.1	13.2
L	0.9	−1.7	−1.3	−1.0
XL	2.3	0.1	−	−
2XL	0.4	0.1	0.1	0.1

Production in relation to water mass was estimated for all size groups based on the method by Zhou et al. (2010). First, production was calculated for each data point along the transect, and secondly mean production within the different water masses (ArW, AtW, PFW, and MW) was computed by averaging production estimates from those data points where salinity and temperature matched the characteristics of the respective water masses.

2.7. Estimating mortality and population change rates

Zhou et al. (2010) derived a very simple equation to estimate mortality within a time period t based on in situ observations of biomass spectra. Number-specific mortality (μ, day^{-1}) is given by

$$\mu(w, t) = gS \qquad (6)$$

where S is the slope of the biomass spectrum (Zhou et al., 2010, their equation 24) The slope of the biovolume spectrum can be used analogously because the specific ratio between biomass to biovolume is cancelled between numerator and denominator when computing the spectra. Based on the observed biovolume spectra and Eq. (6), we estimated mortality rates for the different mesozooplankton size groups (Table 3) and the different water masses at the Polar Front. First, we computed the slope for the 5 different size groups (S: 0.25–0.6 mm ESD, M: 0.6–1 mm ESD, L: 1–2 mm ESD, XL: 2–4 mm ESD and 2XL: 4–10 mm ESD; Table 3) and the four different water masses (described below) by fitting linear regression lines to the data. Secondly, mortality was computed following Eq. (6) by multiplying weight-specific growth g (Eq. (5)) with the appropriate slope. Similar to production estimates (Eq. (3)), population loss L, normalised by size bin, was computed:

$$L = \mu * w * N/dw \quad \left(\text{in mg C m}^{-3}\text{d}^{-1}\right). \qquad (7)$$

Combining Eqs. (5) and (6), we analysed population dynamics by computing the total change in C d^{-1} within the mesozooplankton community, i.e. the population rate, as

$$\text{Population rate} = (g + \mu) * w * N/dw \quad \left(\text{in mg C m}^{-3}\text{d}^{-1}\right) \qquad (8)$$

Table 5

Sensitivity analysis of modelled growth rate estimates for mesozooplankton in relation to different conversion ratios applied. The conversion ratios that were used in the models presented in figures and text are printed in bold. C/Bv = carbon/body volume, C/Chl a = carbon/chlorophyll. Refer to the Methods section for a description of the growth models.

Ratio		Change in ratio	Change in growth rate
C/Bv	**0.0475**	–	–
C/Bv	0.02375	−50%	+22%
C/Bv	0.04275	−10%	+3%
C/Bv	0.05225	+10%	−3%
C/Bv	0.07125	+50%	−22%
C/Chl a	**50**	–	–
C/Chl a	25	−50%	−44%
C/Chl a	75	+50%	+37%
C/Chl a	100	+100%	+69%

3. Results

3.1. Hydrography and distribution of chl a

The physical oceanography at the Polar Front in August 2007 is described in detail by (Våge et al., 2014–this volume), here we will present a brief overview. The frontal system in the study area consisted of the true Polar Front where the cold ArW (T < 0 °C, S < 34.8) and warmer AtW (T > 3 °C, S > 35.0) met throughout the water column below ca. 35 m, and a surface front where a tongue of low saline MW (T > 0 °C, 34.2 < S < 34.8) met with the more saline AtW in the upper ca. 35 m (Loeng, 1991). The AtW was observed in the southern part of the transects from the surface down to the bottom, the ArW in the northern part of the transects below ca 40 m, the PFW (34.8 < S < 35.0) in the central part of the transects, and the MW occupied the northern part of the transects, in the upper ca. 40 m. The MW was more saline than the melt water (S < 34.2) described by Loeng (1991), but this might have been because 2007 was a year of relatively low ice so that there was less melted ice available to reduce the salinity.

The Polar Front was marked by the strong gradients in temperature and salinity across short distances, which were observed by the high-resolution sampling of the instruments mounted on the Scanfish (transect 1 shown in Fig. 2). In the AtW surface maxima of chl a reached values up to 2.8 mg chl a m^{-3}, while in the ArW lower values and subsurface maxima were observed (Fig. 2, bottom). Virtually no chl a was detected in PFW and in MW.

3.2. Mesozooplankton community and distribution

3.2.1. Community structure inferred from net samples

There were clear differences in the composition of the mesozooplankton community across the Polar Front (Table 2). Indicator species for the AtW (*Parasagitta elegans* and *Oithona spinirostris*) and ArW (*Limacina helicina*) were mainly restricted to the respective water masses. In the ArW *P. elegans* was replaced by another, unidentified chaetognath. In the PFW *Fritillaria* sp. reached abundances >200 ind. m^{-3}, and at the Polar Front station C large *Oikopleura* spp. were also observed. In addition to the small-particle feeding appendicularians, the omnivore *Metridia* species (mostly *M. longa*) had elevated abundances at the front stations C, H and I. Carnivore hydrozoans (mostly *Rathkea octopunktata* and *Aglantha digitale*) and Ctenophora larvae were most common in the upper 25 m at the shallow front, i.e. in the MW. Of the *Calanus* species, both *C. finmarchicus* and *C. glacialis* were found at all stations, while the larger copepod *C. hyperboreus*, which is associated with oceanic waters and therefore occurs in deeper waters in the Barents Sea, was rare in the Multinet samples. In the net samples virtually no females of *Calanus* spp. were observed, and the older stages CIV and CV of *C. finmarchicus* and *C. glacialis* were concentrated in the deeper layers and had filled up their lipid reserves. Those older *Calanus* spp. that were located in surface waters at the front were in bad condition and had nearly no lipids. No
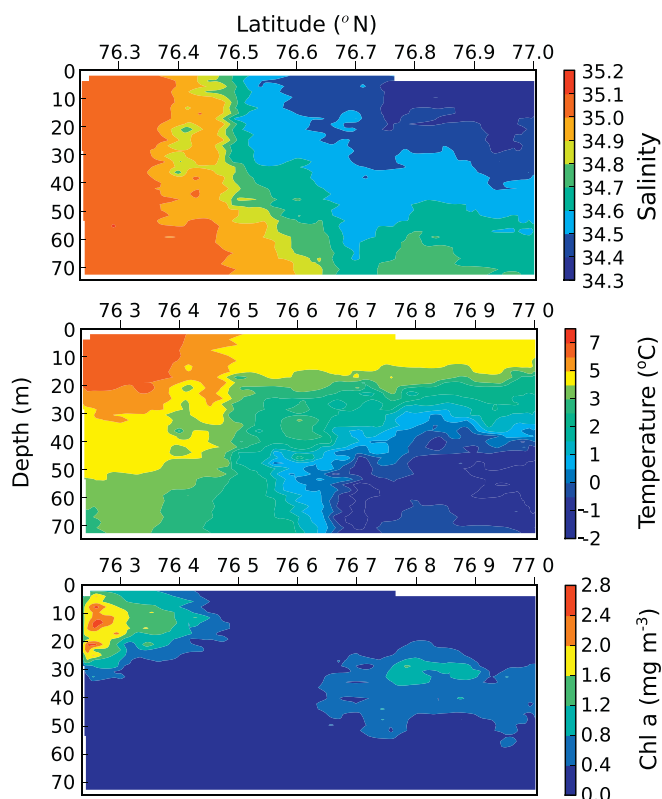
Fig. 2. Transect of salinity (upper panel), temperature (middle panel) and chl *a* (lower panel) across the Polar Front from Hopen Trench (left end of figure) to Barents Sea, in August 2007. Sampling was carried out by the Scanfish–CTD–F–LOPC that undulated in the upper 75 m, see Methods.

Fig. 3. Zooplankton transects across the Polar Front from Hopen Trench (left end of figure) to Storbanken, Barents Sea, in August 2007. Upper panel: small (0.5–1 mm ESD), transparent (AI < 0.4) particles. Middle panel: larger (1–2 mm ESD), transparent particles. Lower panel: larger, more opaque (AI > 0.4) mesozooplankton (MZP). Sampled by a LOPC mounted on the Scanfish that undulated in the upper 75 m. Black triangles mark the locations where Multinet samples were taken. A colour version of this figure is available online.

dormant *Calanus* spp. were observed in the net samples. Young *Calanus* spp. copepodites were concentrated in the upper 50 m at the Arctic station over Storbanken (Station D).

3.2.2. Distribution across the Polar Front inferred from LOPC

The high-resolution sampling revealed marked differences in zooplankton distributions across the front. The Polar Front was characterised by high abundances of small to medium-sized particles (0.5–1 mm ESD). Transparent particles (AI < 0.4) were concentrated in the PFW (Fig. 3 top), likely these particles consisted to a large degree of appendicularians and their houses as discussed in the Methods section. The more opaque (AI > 0.4), small to medium-sized particles, i.e. mainly small, omnivore copepods and *Pseudocalanus* (Table 3), were also concentrated in the PFW near the central part of the transects. Their distribution was very similar to that of the small, transparent particles (data not shown). Very low abundances of the small to medium-sized particles were observed in the AtW and ArW.

A patch of abundant large, transparent particles (chaetognaths and maybe hydrozoans, Table 3) was observed in the AtW at the surface close to the shallow front (Fig. 3). The more opaque, large particles (1–2 mm ESD), i.e. CIV–CVI copepodites of *Calanus* spp., were found at and below the chl *a* maximum in the AtW and ArW (Fig. 3). The larger part (1.5–2 mm ESD) of this group was observed almost exclusively below the chl *a* maximum in the ArW.

In general, zooplankton were most opaque in the ArW, where also a higher proportion of large zooplankton was observed (Fig. 4). In the other water masses, the majority of particles counted by the LOPC were relatively transparent. In the PFW and MW, very few particles with an attenuation index >0.4 were observed.
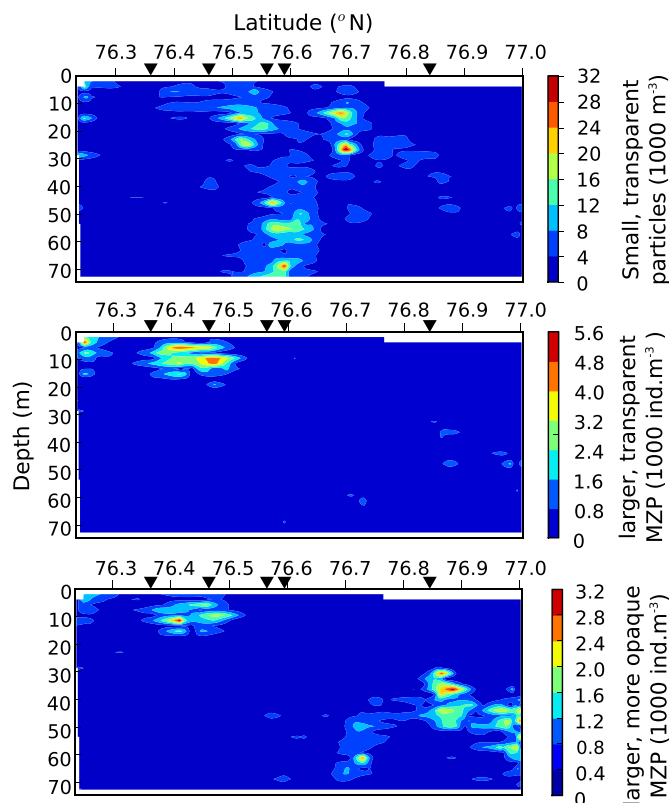
3.3. Biovolume spectra

The biovolume spectrum of the AtW had the highest intercept (2.46), followed by the spectrum of the ArW (2.32). The biovolume spectrum of the PFW had an intercept of 2.29, and the spectrum of the MW was characterised by the lowest intercept (2.13), (Fig. 5). In contrast to the slopes from the PFW (−0.92) and MW (−1.03), slopes from the AtW (−0.71) and ArW (−0.78) were flatter. Based on the slopes, the AtW and ArW could be characterised as systems with a high amount of energy recycling within the mesozooplankton community. The slopes of the PFW, and especially the MW, were indicative of a system with a higher loss of energy from the mesozooplankton community. A remarkable feature of the biovolume spectrum from the ArW was the positive deviation from a straight line spectrum from the S to XL size group (Fig. 5). A positive deviation from the slope in the range from XL to 2XL was noteworthy in the spectrum of the AtW.

3.4. Growth, mortality and population rates

3.4.1. Comparing estimates of Hirst and Bunker (2003) and Zhou et al. (2010)

Weight-specific growth estimated by the empirical fits of Hirst and Bunker (2003) (Eq. (4)) was similar to the growth estimated using the equation derived by Zhou et al. (2010) (Eq. (5), Fig. 6). Using the latter's method, maximum rates of 0.4 d^{-1} were computed for size group L in the AtW (see below), while maximum rates of 0.36 d^{-1} were obtained when using the former's (Supplementary Fig. 1). In the chl *a* patch in the ArW the situation was reversed, with slightly higher rates being computed using Hirst and Bunker (2003). However, in
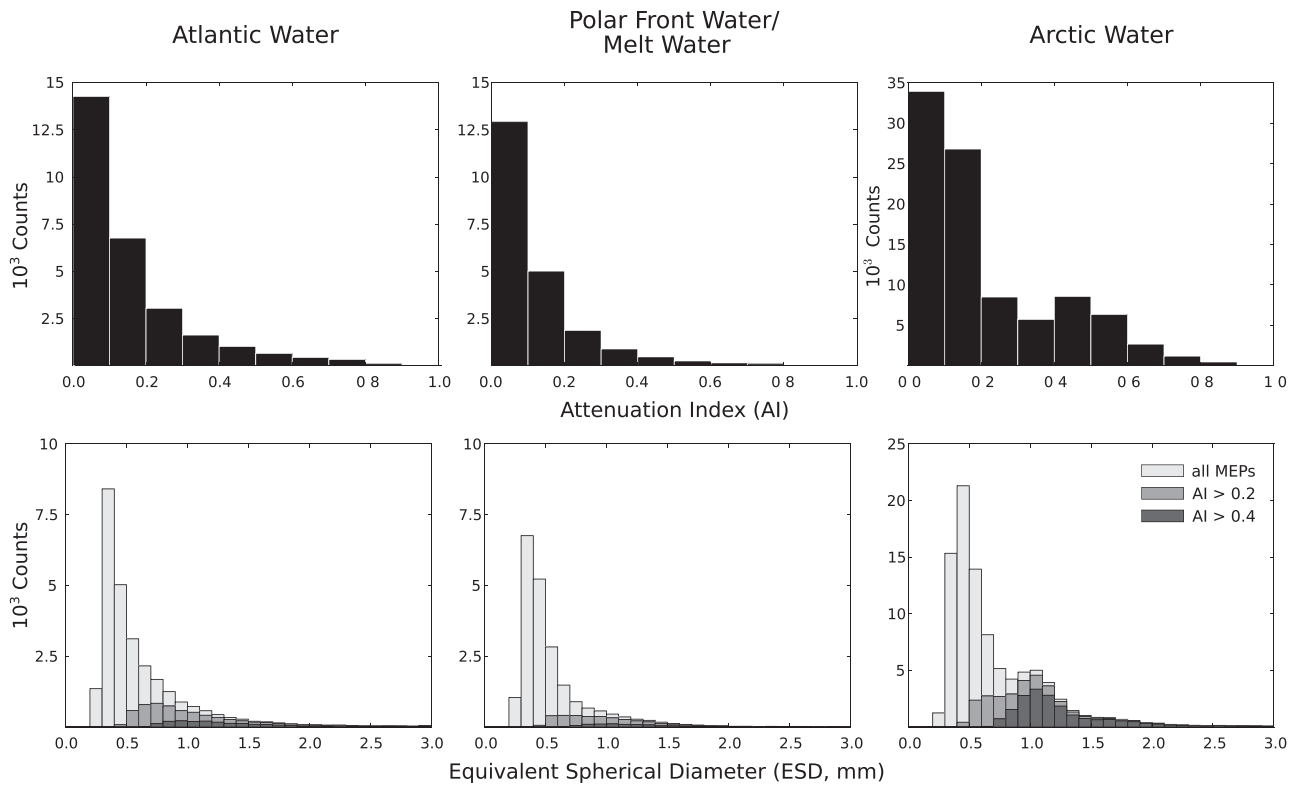
Fig. 4. Sizes and transparencies of Multi-Element-Particles (MEPs) counted by a LOPC in waters at the Polar Front, Barents Sea, in August 2007. Upper panel: histogram of counts vs. attenuation index (AI). The AI ranges from 0 to 1, with 0 being completely transparent and 1 completely opaque particles. Lower panel: Counts of MEPs with different transparencies vs. the size of the particles. Panels from the left to right represent the Atlantic Water, water at the Polar Front and Melt Water, and the Arctic Water, respectively.

general the spatial patterns of zooplankton growth were comparable between these two methods.

3.4.2. Growth and production

The estimated weight-specific growth rates were highest in the upper 30 m on the Atlantic side of the front (Fig. 6). The distributional
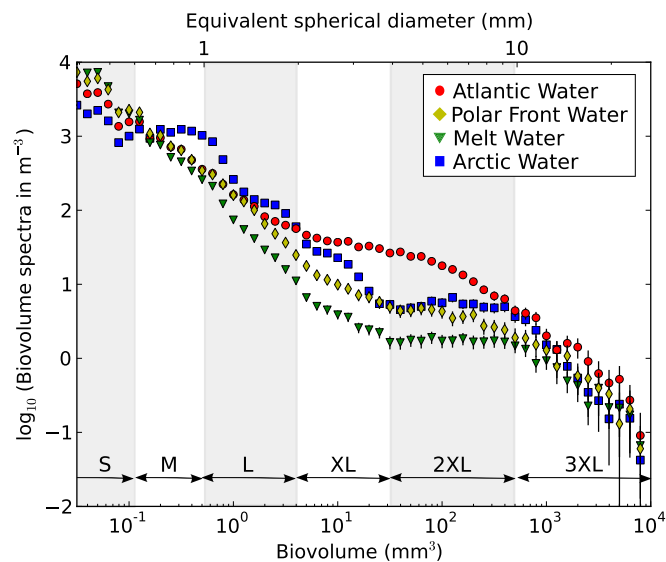
Fig. 5. Biovolume spectra (markers) and 95% confidence intervals (black bars) of the mesozooplankton community in different water masses at the Polar Front in the Barents Sea. Based on data collected in the upper 75 m during August 2007. The size ranges of the 6 size groups (S to 3XL) analysed in this study are given for comparison, see Table 3 for the main species within each size group. A colour version of this figure is available online.

pattern of weight-specific growth rates indicates the potential growth if plankton were equally distributed along the transect, but it is the production that shows where most mesozooplankton growth took place. Also the estimated mean specific production (normalised by weight) was highest in the AtW, especially in the upper layer, and lowest in the ArW (Fig. 7, Table 4). The secondary production estimated for the whole mesozooplankton community from S to XL size groups at the Polar Front was up to 14 g C m^{-3} d^{-1} (Fig. 6, Table 3). The small size group contributed most to this high secondary production in the central part of the transect at the front. Compared to the production of the small size group, that of size groups L and larger was very low. In ArW, however, a relatively low production was computed for the S size group (Fig. 7).

For large *Calanus*, weight-specific growth reached maximum values of 0.4 d^{-1} in the AtW, but were low in the other water masses due to low temperatures and/or low chl *a* concentrations (ref. Fig. 2). Weight-specific growth rates for the other size groups showed the same spatial pattern along the transect owing to the prominent effect of temperature and chl *a* in estimating the rates. For all size groups, positive growth only occurred in a few patches along the transect, therefore spatial averages of weight-specific growth rates were low (data not shown). For CIV, CV and adult *Calanus* the growth rates were lowest in the ArW (around 0.002 d^{-1}), slightly higher (0.005 d^{-1}) in the PFW and MW, and highest (0.01 d^{-1}) in the AtW.

Throughout most of the study area, the estimated production of older stages of *Calanus* spp. was low (Fig. 6), even at the chl *a* maximum in the ArW, where high abundances of older stages of *Calanus* were observed by the LOPC, due to a low "potential growth" (Figs. 3, 6). The "potential growth" was high in near surface waters in the AtW and at and above the chl *a* maximum in the ArW and MW. Nearly no large *Calanus* were found above the chl *a* maximum on the Arctic side of the front, so that noticeable production of older stage *Calanus* was only observed in the upper 30 m in AtW. In patches the production of older stage *Calanus*
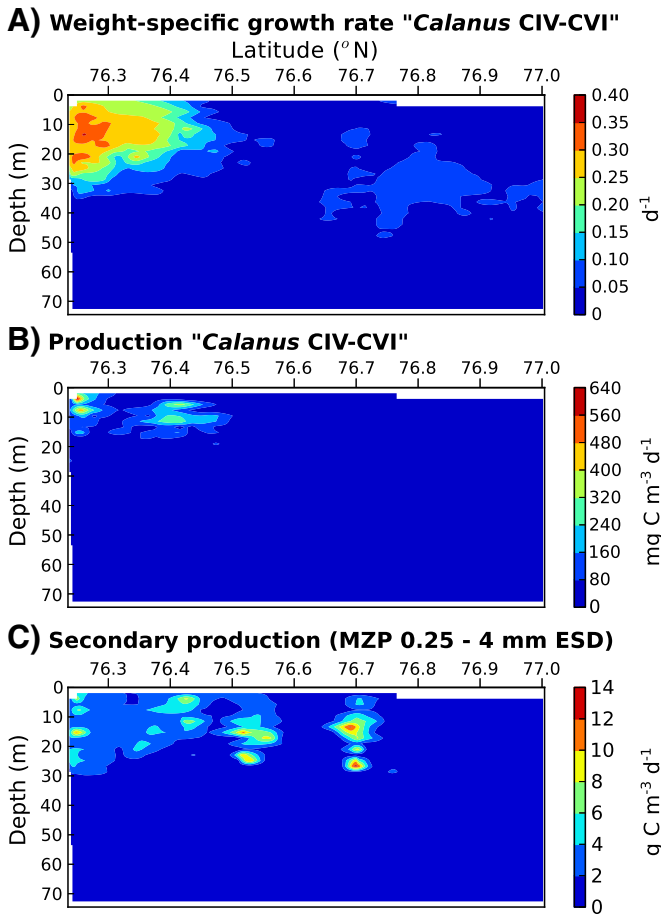
Fig. 6. Growth and production. Estimated based on semi-empirical fits to temperature and chlorophyll *a* and on biomass spectrum theory (Zhou et al., 2010). Upper panel: weight-specific growth rate within the size interval 1–2 mm ESD (mainly *Calanus* spp. CIV, CV and adults, Table 3). Middle panel: production within the same size interval. Lower panel: production of the mesozooplankton (MZP) community between 0.25 and 4 mm ESD (size groups S–XL, Table 3). All estimates based on data collected along a transect crossing the Polar Front in August 2007, applying Eqs. (5) and (3), and a carbon:chlorophyll *a* ratio of 50. A colour version of this figure is available online.
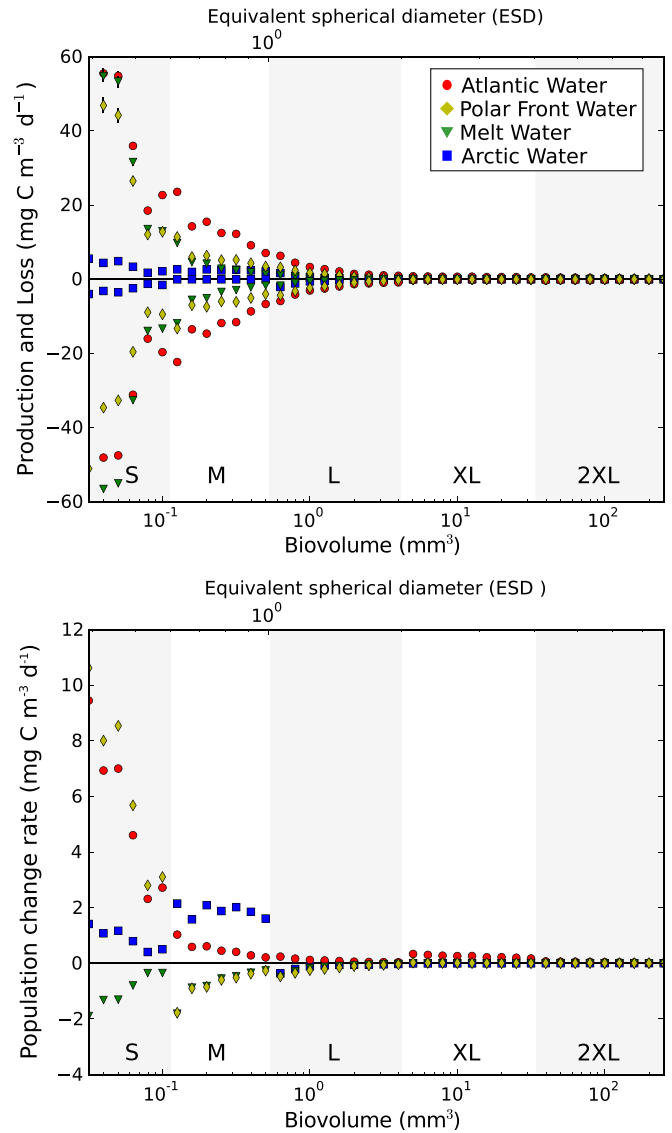

Fig. 7. Growth, mortality and population change rates for the mesozooplankton at the Polar Front, Barents Sea, August 2007. Separated by the different water masses. Upper panel: growth and mortality. Lower panel: population rate. A colour version of this figure is available online.

was > 300 mg C m^{-3} d^{-1}, significantly higher than the average production of 23.4 mg C m^{-3} d^{-1}, or ca. 1.8 g C m^{-2} d^{-1}, for CIV–CVI *Calanus* in the AtW. At the chl *a* maximum in the ArW, a moderate production of the M size group (mostly CI–CIII *Calanus* spp. and *Pseudocalanus*) was observed, ca. 50 mg C m^{-3} d^{-1} (data not shown). Relative to an exponential decrease with size, the production of the M size group was elevated in the ArW (Fig. 7).

Compared to the other water masses, relatively high production rates were computed for the XL and 2XL size groups in the AtW (Fig. 7, Table 4). Production estimated for the zooplankton community in MW showed no distinct pattern, and decreased exponentially with size.

3.5. Mortality and population change rate

The spatial patterns of mortality and population loss rates were very similar to the patterns of growth and production, due to the close relationship between growth and mortality (Eq. (6)), however, some differences emerged because of the heterogeneity in growth and in the slopes of the biovolume spectra along the transect. Because of the close relationship between growth and mortality, data on mortality are presented in the supplementary material available online (Supplementary Fig. 2). Number-specific mortality rates were highest in the upper 30 m at the southern edge of the transect in the AtW and MW, −0.35 d^{-1} for the size range of CIV–CVI *Calanus* and −1.2 d^{-1} for the whole mesozooplankton community. Relatively high mortality rates were

also computed for the layer above the chl *a* maximum in the ArW, −0.1 d^{-1} for the size range of older stage *Calanus*, and −0.5 d^{-1} for the whole mesozooplankton community. Population loss rates of older *Calanus* were estimated to be highest at the shallow front in the upper 30 m of the MW and AtW (−150 to −550 mg C m^{-3} d^{-1}), and relatively low along the rest of the transect. The maximum population loss of mesozooplankton between 0.25 and 4 mm was around −14 g C m^{-3} d^{-1}, in the MW at the central part of the Polar Front.

Population change rates, in C m^{-3} d^{-1} (Eq. (8)), were computed for all size groups, and are shown for the size groups M and L, and for the combined mesozooplankton size groups S–XL (Fig. 8). The population change rate of the XL and 2XL size group is shown in Supplementary Fig. 3. In the AtW, positive population rates were estimated for all size groups (Fig. 7). Compared to the other water masses, relatively high rates were estimated for the XL and to a lesser degree also for the 2XL size group in the AtW (Table 4). For all size groups, negative or very low population rates were observed in the MW.

The population rates of the whole mesozooplankton community were completely dominated by the S size group, so that the bottom panel of Fig. 8 virtually depicts the population rates of the S size

group. The production of this group, consisting mainly of *Oithona* and *Fritillaria*, was an order of magnitude higher than that of the M and L size groups, which consisted mainly of medium- to large-sized copepods (Fig. 7, Table 4). An increase in the population of about 130 mg C m^{-3} d^{-1} was estimated for the S size group in the AtW and PFW (Fig. 7, Table 4). The S size group was also the only size group with positive population rates in the PFW (Table 4).

For the M and L size groups small, positive population change rates were estimated in the AtW, and negative rates (up to −3 mg C m^{-3} d^{-1}) in the PFW and MW (Figs. 8, 7, Table 4). Negative population change rates were also estimated for the L size group in the ArW, but for the M size group (mainly *Pseudocalanus* and *Calanus* CI–CIII, Table 3) a production of ca. 13 mg C m^{-3} was estimated in the ArW (Table 4). The highest population rate of the M size group (up to 160 mg C m^{-3} d^{-1}) was computed for zooplankton patches within the chl *a* maximum in the ArW, where high abundances of CI–CIII copepodites of *Calanus* were observed by both the LOPC (data not shown) and live samples (Table 2). In two distinct patches in the AtW at the shallow front very low population change rates were estimated for the M size group (Fig. 8, top). Highly negative population rates (−100 mg C m^{-3} d^{-1}) were also estimated for the L size group (mainly CIV–CVI *Calanus*, Table 3) for the patches in MW at the shallow front (Fig. 8, centre). In these patches high abundances of large, transparent particles were observed by the LOPC (Fig. 3) and live samples also revealed high abundances of chaetognaths and carnivore hydrozoans (Tables 2, 3).

The population change rates estimated for the combined XL and 2XL size groups (most likely euphausids) were low along most of the transect (Table 4, Supplementary Fig. 3), though in the AtW at the southern edge of the transect highly positive population rates of up to 80 mg C m^{-3} d^{-1} were computed for the upper 30 m. These positive population rates did not coincide with the highly negative population rates computed for the M and L size groups in that area, but were located farther south along the transect. The only size group within the patches close to the shallow front in the MW with positive population rates was the S size group (Fig. 8).

4. Discussion

We presented data on zooplankton growth, mortality and production with high spatial resolution along a transect crossing the Polar Front in the Barents Sea. The rates were estimated based on field data and biovolume spectrum theories, and our study may be the first presentation of vital zooplankton rates at such high spatial resolution with in situ environmental data of equally high-resolution. Significant differences in growth and production rates between water masses were observed, produced by spatial variations of hydrography, chl *a*, and the size-specific distribution of zooplankton across the front.

4.1. Quality control and uncertainty estimates

4.1.1. Quality control of LOPC data

The quality check of data measured by the LOPC revealed that for the most part the data were of excellent quality, but in the PFW some irregularities appeared. A low percentage (0.1%) of faulty registrations of MEPs were observed in the PFW. The reason for this is unknown at present, but may have been due to a computer process unit memory overload of the LOPC in waters with high turbidity (Schultes and Lopes, 2009), and also possibly in relation to the multiplexer of the deck unit of the LOPC (Ley Sullivan, Brooke Oceans, pers. comm.). Though high abundances of particles were observed in the PFW they were far below the limit of 10^6 m^{-3} given for the LOPC (Herman et al., 2004). Also in a frontal zone in the California Current faulty data were detected, on average 0.5% of all MEPs (Ohman et al., 2012). The few irregularities observed in the four data files from the central parts of the Polar Front were examined and did not affect subsequent data analyses. In the AtW and ArW no faulty data were observed, and in the ArW the waters were especially clear with low numbers of small particles. In combination with the high abundances of large copepods in the ArW, this resulted in low TC/MEP ratios, which in our case did not indicate any false counts as in Schultes and Lopes (2009), but rather identified a blue water situation in the ArW.

4.1.2. Uncertainty in estimates of vital rates

The Polar Front, i.e. the PFW and MW in the central parts of our study area, was characterised by very low chl *a* values, high abundances of small (<1 mm ESD) zooplankton (both opaque and transparent) and by relatively steep slopes in the biovolume spectra, indicative of a high loss from the upper 75 m. If disintegrated, discarded houses of appendicularians were counted in the S size group, this would lead to a steeper slope and a higher intercept in the spectra than in reality. Loss rates then would be overestimated, and population change rates would be underestimated. In the PFW and MW other factors contributed to uncertainty also in estimates of growth and production. First, carbon content of appendicularians is relatively low and the conversion factor from biovolume:C of 0.0475, which was applied, certainly would overestimate their carbon content (Sato, 2003). Reducing the conversion factor by 50%, the growth estimates would be raised by 22% due to higher growth at lower body size (Table 5). Second, the growth estimates were based on equations tailored to copepod growth, while vital rates of appendicularians can be an order of magnitude

A) Population rate size group M

B) Population rate "*Calanus* CIV-CVI"
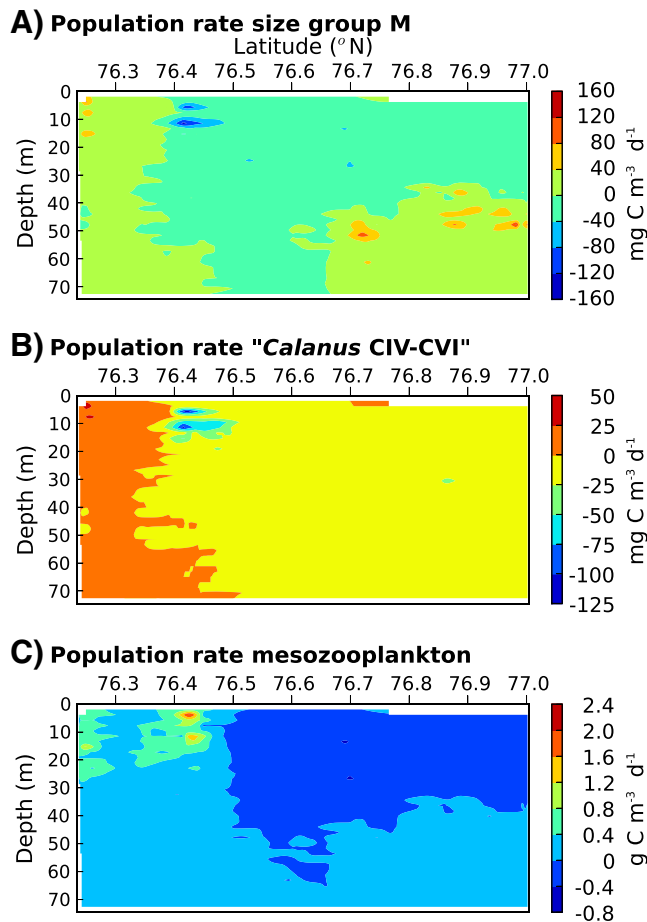

C) Population rate mesozooplankton

Fig. 8. Population change rate. Estimated based on mesozooplankton data collected with a LOPC at the Polar Front in August 2007. Upper panel: population rate for the M size group (see Table 3 for species composition). Middle panel: population rate for the L size group. Lower panel: population rate for the mesozooplankton community between 0.25 and 4 mm ESD (size groups S–XL, Table 3). A colour version of this figure is available online.

higher (Lopez-Urrutia et al., 2003). Both these factors point to an under-estimation of growth and production of appendicularians in the PFW.

For a copepod-dominated community, a higher C:biovolume conversion factor might be more realistic (Forest et al., 2011). This would indicate an overestimation of growth for the copepod-dominated community in the AtW and ArW, and for the large fraction of small copepods in the PFW (Table 5). The combined abundance of *Oithona similis* and juvenile *Pseudocalanus* spp. was higher than that of appendicularians at the front from live samples collected by the 180-μm net, which typically undersamples small copepods (e.g. Gallienne and Robins, 2001). These copepods therefore contributed most to the growth and production estimates for the S size group, and in general, at the Polar Front. Andersen et al. (2011) compared measured growth rates of the copepod community in the Sargasso Sea with estimates by Hirst and Bunker (2003), and found that the measured rates were ca. 20% lower than the estimates. Our growth estimates were 10% less than the maximum growth estimates based on Hirst and Bunker (2003), indicating a slight overestimation of growth.

In principal, it might also be possible to estimate the carbon content of zooplankton particles based on their transparency (AI), when assuming that darker material (e.g. lipids) is more carbon-rich than transparent material like new appendicularian houses. This would require a comparison of carbon measurements of particles sensed by the LOPC with the AI distribution of these particles. To make the comparison statistically sound, a large number of measurements from different zooplankton communities would be required. Such a study could be very useful for increasing the precision in estimating growth rates, and also for estimating carbon flux based on LOPC data.

No *Calanus* spp. in dormancy were observed in the net samples, but some *Calanus* might already have entered diapause during our study in August (Tande, 1989). The sampling with the LOPC was restricted to the upper 75 m, so that those copepods that might have overwintered at depth did not influence the estimates of growth and mortality based on biovolume spectrum theories.

We used a C:chl *a* conversion factor of 50 for all data. A higher factor of 75 might have been more realistic as discussed by Pesant et al. (1998). They point out that under conditions found at high-latitudes, i.e. continuous light but low temperature limiting phytoplankton growth, the carbon content in phytoplankton cells is higher than that of temperate areas with relatively short daylight and high temperatures. They therefore applied a conversion factor of 75 to their data. Growth estimates in our study would have been ca. 40% higher using a conversion factor of 75 (Table 5). Especially in the AtW and ArW, where higher chl *a* concentrations were observed than those of the PFW and MW, the growth may have been underestimated by about 40% due to the C:chl *a* ratio used. Combining over- and underestimates for the copepod community ($+25\%$, $+10\%$, -40%), the deviation is significantly less than the variations of growth rate estimates compiled by Hirst and Bunker (2003), which are about 1 to 2 orders of magnitude.

This indicates that the growth and production estimates from the AtW and ArW, where the mesozooplankton community was dominated by copepods, were realistic, while estimates from PFW and MW, where a high proportion of appendicularians occurred, were afflicted with greater uncertainty and likely underestimated.

4.2. Mortality

The specific mortality rates computed by multiplying specific growth rates with the slope of the biovolume spectrum (Eq. (6)) agreed very well with rates estimated for copepods by other methods (Eiane and Ohman, 2004; Ohman et al., 2004), and thereby strongly support the applicability of the simple method developed by Zhou et al. (2010) for estimating mortality rates. Relatively high specific mortality rates (-0.35 d^{-1}) were estimated for a patch of CIV, CV and adult *Calanus* spp. in the AtW, where chaetognaths and hydrozoans as possible predators were observed. This is equivalent to the upper limit of the

confidence interval estimated for mortality of *C. finmarchicus* CV in a Norwegian fjord dominated by visual predators (Eiane et al., 2002) and corresponds to the high rates on the Icelandic shelf in June (Gislason et al., 2007) and in an Arctic fjord (Arnkværn et al., 2005). The mortality rates estimated based on Eq. (6) incorporate all losses from the system, in our case the upper 75 m of the pelagic layer, i.e. natural mortality, predation mortality and a loss through downward migration. Most older stage *Calanus* in the AtW were located at depth, and the ones in surface waters were noted to be in poor condition. Presumably therefore the high mortality rates estimated for older stage *Calanus* in the AtW were due to a combination of multiple causes including more predator species, increased natural mortality, and a higher downward migration. Throughout most of the transect across the front specific mortality rates for older stage *Calanus* spp. varied between 0 and -0.15, which is in good agreement with the range estimated for these developmental stages (Eiane et al., 2002; Ohman et al., 2004). Mortality rates for the other mesozooplankton size ranges in our study varied mainly between 0 and -0.15 as well, comparable to rates estimated e.g. for *Oithona* sp. and *Pseudocalanus* sp. (Eiane and Ohman, 2004; Hirst and Ward, 2008).

The spatial pattern of mortality exhibited considerable variability along the transect from the AtW to ArW, and strongly influenced population rates. In contrast to earlier studies our results are based on measured high-resolution environmental data, and they confirm the high spatial variability in mortality that has been predicted for *Calanus* spp., both by recent models extrapolated from lower-resolution field data (Ohman and Hsieh, 2008; Plourde et al., 2009), and by a high-resolution biophysical model (Skarðhamar et al., 2011).

4.3. Growth, production and population change rates

We estimated very high secondary production for some patches at the Polar Front (up to 14 mg C m^{-3} d^{-1}), but average production was highest in the AtW. This is in line with the general perception that the AtW is the most productive water mass in the Barents Sea (e.g. Reigstad et al., 2011). In the AtW also the XL and 2XL size groups contributed to production, in addition to the size groups S, M and L. The larger size groups XL and 2XL likely contained mostly euphausids, and their average production was estimated 8.9 mg C m^{-3} d^{-1}. For these mobile animals that are capable of horizontal and vertical migrations (Klevjer and Kaartvedt, 2011), however, production estimates may also include migration into the study area and the sampled depth range. Likewise, the considerable loss that was estimated for the 2XL size group may have been due to migrating euphausids that left the sampled water volume.

While high abundances of large copepods were observed on either side of the Polar Front, the abundance at the central front was dominated by small mesozooplankton and nearly no large copepods were found here. Søreide et al. (2003) observed the same tendencies in macrozooplankton abundance along a transect from Hopen trench towards Storbanken in March and May 1999. Mixed waters near the front were characterised by very low abundances of macrozooplankton, while high abundances were observed in the ArW and AtW. There is no a priori reason why larger zooplankton should not occur in the frontal zone. The high production of small zooplankton at the front may indicate that large zooplankton like *Calanus* were outcompeted by *Oithona* and appendicularians.

The estimated production of the small-size zooplankton, consisting mainly of *Oithona* spp. and *Fritillaria* sp., was an order of magnitude higher than the production by all other size groups combined, including large copepods. Very high production was estimated at the Polar Front (in the MW and PFW), but also in the AtW. In these water masses the average production of the small size group was estimated to be around 1 g C m^{-3} d^{-1}. Few production estimates for small copepods and appendicularians exist in the literature, partly because of frequent undersampling of this group. Based on the results on high growth of

small-sized plankton (e.g. Hirst and Bunker, 2003), and on high abundances often observed (e.g. Gallienne and Robins, 2001), the high production rates estimated from our high-resolution in situ data set for small zooplankton at the Polar Front seem realistic. Elevated abundances of appendicularians have been observed at fronts and in regions with strong gradients elsewhere (Andersen et al., 2011; Forest et al., 2011), and ocean fronts can be regions of enhanced productivity by pico- and nanoplankton, which is efficiently retained by *Oikopleura* spp. and *Fritillaria* spp. (e.g. Deibel and Lee, 1992; Riemann et al., 2011). From our data set also high loss rates were estimated for the small size group in the AtW, PFW and MW. In the MW this led to negative population change rates, despite high production. As discussed earlier, loss rates may have been overestimated if fragmented houses of appendicularians were counted in the small size class. However, the question arises by whom the produced biomass in the small size-class is utilised. The production of appendicularian houses can increase export production dramatically (Berline et al., 2011), and therefore an important amount of carbon might have been channelled to the benthos. Appendicularian houses are also important for recycling of material in the pelagic zone (Ploug et al., 2008), and both appendicularians and small copepods are important food sources for fish larvae (Gorsky and Fenaux, 1998; Turner, 2004). During our study, capelin (*Mallotus villosus*) was segregated in size classes at the front, with smaller capelin feeding in the PFW and MW, and larger animals in the ArW (Drinkwater et al., unpublished results). These preliminary results may indicate the importance of the Polar Front as a nursery ground for capelin.

The pattern that emerged for the well-studied *Calanus* spp. community at the Polar Front is consistent with earlier results, but this study is to our knowledge one of the first that presents estimates of vital rates based on high-resolution measurements in the field (see also Basedow et al., 2010b; Zhou et al., 2009). The data set reveals the high degree of patchiness in production, which had been anticipated based on earlier sampling with lower resolution. In the AtW the population was centred around older stages (CIV–CV) in poor condition, while in the ArW high abundances of CI–CIII copepodites were observed. The production of CIV–CV in AtW was estimated to be 23 mg C m^{-3} d^{-1}, and the production of CI–CIII and some older stage *Pseudocalanus* in the ArW was around 17 mg C m^{-3} d^{-1}. This is in agreement with known production estimates and population development of *Calanus* spp. at the Polar Front, where the production of CI–CIII stages of t*C. glacialis* was modelled to peak in mid August, i.e. during the time of our study, with ca. 150 mg C m^{-2} d^{-1} (Slagstad and Tande, 1990; Tande, 1989). The same bio-energetic model predicts a maximum production of *C. finmarchicus* in mid-July, of both CIV–CVs and CI–CIIIs, and a decreasing production thereafter (Tande, 1989). At the time of our study substantial population growth (13.2 mg C m^{-3} d^{-1}) of the *Calanus* spp. community was observed only in the ArW, because of the high loss of older stages in the AtW, and the low mortality of younger stages in the ArW. Our results from the field are also comparable to the maximum production rates of ca. 150 mg C m^{-2} d^{-1} that were obtained from modelling the mesozooplankton community in the ArW in the Barents Sea (Reigstad et al., 2011).

4.4. Conclusions

The vital rates that were estimated based on high-resolution field data and on biovolume spectrum theories agreed generally well with purely empirically estimated rates, and with those of the literature. The processes seen in high spatial resolution by the LOPC were confirmed by the taxonomic composition of the zooplankton community from net tow live samples. This study has demonstrated the great potential of using high-resolution automated sampling in combination with station-based sampling and biovolume spectrum theories to yield realistic in situ rates and patterns (see also Basedow et al., 2010b).

The spatial patterns of production across the Polar Front showed a distinct patchiness and distinct characteristics of the different water masses:

- ArW was characterised by subsurface maxima of chlorophyll, and an estimated population growth of ca. 13 mg C m^{-3} d^{-1} of CI–CIII *Calanus* spp. and some older stage *Pseudocalanus* within the chl *a* maximum.
- PFW and MW were characterised by low chl *a* concentrations, but high abundances and high production of around 1 g C m^{-3} d^{-1} of small copepods (*Oithona* spp.) and appendicularians (*Fritillaria* sp.). The high loss rates (-166 to -271 mg C m^{-3} d^{-1}) of small zooplankton may contribute a substantial amount of carbon to the benthos and to pelagic predators like young capelin.
- AtW was the most productive water mass, with surface chl *a* maxima and an estimated population growth of 134 mg C m^{-3} d^{-1} of small zooplankton, 3.6 mg C m^{-3} d^{-1} of medium-sized copepods and 0.9 mg C m^{-3} d^{-1} of CIV–CVI *Calanus*. For those *Calanus* spp. in the surface layer, the estimated specific mortality rates were up to -0.35 d^{-1}, partly due to high predation pressure by hydrozoans and chaetognaths.

Supplementary data to this article can be found online at http://dx.doi.org/10.1016/j.jmarsys.2013.07.015.

References

Aksnes, D.L., Magnesen, T., 1988. A population dynamics approach to the estimation of production of four calanoid copepods in Lindåspollene, western Norway. Mar. Ecol. Prog. Ser. 45, 57–68.

Aksnes, D.L., Miller, C.B., Ohman, M.D., Wood, S.N., 1997. Estimation techniques used in studies of copepod population dynamics — a review of underlying assumptions. Sarsia 82, 279–296.

Aksnes, D.L., Ohman, M., 1996. A vertical life table approach to zooplankton mortality estimation. Limnol. Oceanogr. 41, 1461–1469.

Amante, C., Eakins, B.W., 2009. ETOPO1 1 arc-minute global relief model: procedures, data sources and analysis. NOAA Tech. Memo. NESDIS NGDC 24, 1–19.

Andersen, N.G., Nielsen, T.G., Jakobsen, H.H., Munk, P., Riemann, L., 2011. Distribution and production of planton communities in the subtropical convergence zone of the Sargasso Sea. II. Protozooplankton and copepods. Mar. Ecol. Prog. Ser. 426, 71–86.

Anonymous, 2006. LOPC Software Operation Manual. Brooke Ocean Technology Ltd., Dartmouth, Nova Scotia, Canada.

Arnkværn, G., Daase, M., Eiane, K., 2005. Dynamics of coexisting *Calanus finmarchicus*, *Calanus glacialis* and *Calanus hyperboreus* populations in a high-Arctic fjord. Polar Biol. 28 (7), 528–538.

Basedow, S.L., Edvardsen, A., Tande, K.S., 2006. Spatial patterns of surface blooms and recruitment dynamics of *Calanus finmarchicus* in the NE Norwegian Sea. J. Plankton Res. 28, 1181–1190.

Basedow, S.L., Tande, K.S., Norrbin, M.F., Kristiansen, S., 2013. Capturing quantitative zooplankton information in the sea: performance test of Laser Optical Plankton Counter and Video Plankton Recorder in a *Calanus* sp. dominated summer situation. Prog. Oceanogr. 108, 72–80.

Basedow, S.L., Tande, K.S., Stige, L.C., 2010a. Habitat selection by a marine copepod during the productive season in the Subarctic. Mar. Ecol. Prog. Ser. 416, 165–178.

Basedow, S.L., Tande, K.S., Zhou, M., 2010b. Biovolume spectrum theories applied: spatial patterns of trophic levels within a mesozooplankton community at the polar front. J. Plankton Res. 32, 1105–1119. http://dx.doi.org/10.1093/plankt/fbp110.

Beaulieu, S.E., Mullin, M.M., Tang, V.T., Pyne, S.M., King, A.L., Twinning, B.S., 1999. Using an optical plankton counter to determine the size distributions of preserved zooplankton samples. J. Plankton Res. 21, 1939–1956.

Berline, L., Stemmann, L., Vichi, M., Lombard, F., Gorsky, G., 2011. Impact of appendicularians on detritus and export fluxes: a model approach at DyFAMed site. J. Plankton Res. 33, 855–872.

Bi, H., Rose, K.A., Benfield, M.C., 2011. Estimating copepod stage-specific mortality rates in open ocean waters: a case study from the northern Gulf of Mexico, USA. Mar. Ecol. Prog. Ser. 427, 145–159.

Checkley, D.M., Davis, R.E., Herman, A.W., Jackson, G.A., Beanlands, B., Regier, L.A., 2008. Assessing plankton and other particles in situ with the SOLOPC. Limnol. Oceanogr. 53, 2123–2136.

Daase, M., Eiane, K., 2007. Mesozooplankton distribution in northern Svalbard waters in relation to hydrography. Polar Biol. 30 (8), 969–981.

Deibel, D., Lee, S.H., 1992. Retention efficiency of sub-micrometer particles by the pharyngeal filter of the pelagic tunicate Oikopleura vanhoeffeni. Mar. Ecol. Prog. Ser. 81, 25–30.

Edvardsen, A., Slagstad, D., Tande, K.S., Jaccard, P., 2003. Assessing zooplankton advection in the Barents Sea using underway measurements and modelling. Fish. Oceanogr. 12, 61–74.

Edvardsen, A., Zhou, M., Tande, K., Zhu, Y., 2002. Zooplankton population dynamics: measuring in situ growth and mortality rates using an Optical Plankton Counter. Mar. Ecol. Prog. Ser. 227, 205–219.

Eiane, K., Aksnes, D.L., Ohman, M.D., Wood, S., Martinussen, M.B., 2002. Stage-specific mortality of Calanus spp. under different predation regimes. Limnol. Oceanogr. 47, 636–645.

Eiane, K., Ohman, M.D., 2004. Stage-specific mortality of Calanus finmarchicus, Pseudocalanus elongatus and Oithona similis on Fladen Ground, North Sea, during a spring bloom. Mar. Ecol. Prog. Ser. 268, 183–193.

Forest, A., Stemmann, L., Picheral, M., Burdorf, L., Robert, D., Fortier, L., Babin, M., 2011. Size distribution of particles and zooplankton across the shelf-basin system in Southeast Beaufort Sea: combined results from an Underwater Vision Profiler and vertical net tows. Biogeosci. Discuss. 8, 11405–11452.

Gaardsted, F., Tande, K.S., Basedow, S.L., 2010. Measuring copepod abundance in deep–water winter habitats in the NE Norwegian Sea: intercomparison of results from laser optical plankton counter and multinet. Fish. Oceanogr. 19, 480–492.

Gallienne, C.P., Robins, D.B., 2001. Is Oithona the most important copepod in the world's oceans? J. Plankton Res. 23, 1421–1432.

Gallienne, C.P., Robins, D.B., Woodd-Walker, R.S., 2001. Abundance, distribution and size structure of zooplankton along a 20° west meridional transect of the northeast Atlantic Ocean in July. Deep-Sea Res. II 48, 925–949.

Gislason, A., Eiane, K., Reynison, P., 2007. Vertical distribution and mortality of Calanus finmarchicus during overwintering in oceanic waters southwest of Iceland. Mar. Biol. 150, 1253–1263.

Gorsky, G., Fenaux, R., 1998. The role of appendicularia in marine food webs. In: Bone, Q. (Ed.), The Biology of Pleagic Tunicates. Oxford University Press, pp. 161–169.

Herman, A.W., Beanlands, B., Phillips, E.F., 2004. The next generation of Optical Plankton Counter: the Laser-OPC. J. Plankton Res. 26 (10), 1135–1145.

Herman, A.W., Harvey, M., 2006. Application of normalized biomass size spectra to laser optical plankton counter net intercomparisons of zooplankton distributions. J. Geophys. Res. 111, c05S05. http://dx.doi.org/10.1029/2005JC002948.

Hirst, A.G., Bunker, A.J., 2003. Growth of marine planktonic copepods: global rates and patterns in relation to chlorophyll a, temperature and body weight. Limnol. Oceanogr. 48, 1988–2010.

Hirst, A.G., Kiørboe, T., 2002. Mortality of marine planktonic copepods: global rates and patterns. Mar. Ecol. Prog. Ser. 230, 195–209.

Hirst, A.G., Lampitt, R.S., 1998. Towards a global model of in situ weight-specific growth in marine planktonic copepods. Mar. Biol. 132, 247–257.

Hirst, A.G., Ward, P., 2008. Spring mortality of the cyclopoid copepod Oithona similis in polar waters. Mar. Ecol. Prog. Ser. 372, 169–180.

Holm-Hansen, O., Riemann, B., 1978. Chlorophyll a determination: improvements in methodology. Oikos 30, 438–447.

Hunt, G.L.J., Blanchard, A.L., Boveng, P., Dalpadado, P., Drinkwater, K.F., Eisner, L., Hopcroft, R.R., Kovacs, K.M., Norcross, B.L., Renaud, P., Reigstad, M., Renner, M., Skjoldal, H.R., Whitehouse, A., Woodgate, R.A., 2013. The Barents and Chukchi Seas: comparison of two Arctic shelf ecosystems. J. Mar. Syst. 109–110, 43–68.

Huntley, M.E., Boyd, C., 1984. Food-limited growth of marine zooplankton. Am. Nat. 124, 455–478.

Huntley, M.E., Lopez, M.D.G., 1992. Temperature-dependent production of marine copepods: a global synthesis. Am. Nat. 140, 201–242.

Ikeda, T., Motoda, S., 1978. Estimated zooplankton production and their ammonia excretion in the Kuroshio and adjacent seas. Fish. Bull. 76, 357–367.

Jonasdottir, S.H., Trung, N.H., Hansen, F., Gärtner, S., 2005. Egg production and hatching success in the calanoid copepods Calanus helgolandicus and Calanus finmarchicus in the North Sea from March to September 2001. J. Plankton Res. 27, 1239–1259.

Kimmerer, W.J., 1987. The theory of secondary production calculations for continuously reproducing populations. Limnol. Oceanogr. 32, 1–13.

Kimmerer, W.J., McKinnon, A.D., 1987. Growth, mortality, and secondary production of the copepod Acartia tranteri in Westernport Bay, Australia. Limnol. Oceanogr. 32, 14–28.

Klevjer, T.A., Kaartvedt, S., 2011. Krill (Meganyctiphanes norvegica) swim faster at night. Limnol. Oceanogr. 56, 765–774.

Lalli, C.M., Parsons, T.R., 1997. Biological Oceanography: An Introduction, 2nd edition. Elsevier Butterworth-Heinemann, Oxford, U. K.

Le Borgne, R., 1982. Zooplankton production in the eastern tropical Atlantic Ocean: net growth efficiency and P:B in terms of carbon, nitrogen, and phosphorus. Limnol. Oceanogr. 27, 681–698.

Lindemann, R.L., 1942. The tropho-dynamic aspect of ecology. Ecology 23, 399–418.

Loeng, H., 1991. Features of the physical oceanographic conditions in the Barents Sea. Polar Res. 10 (1), 5–18.

Lopez-Urrutia, A., Acuna, J.L., Irigoien, X., Harris, R., 2003. Food limitation and growth in temperate epipelagic appendicularians (Tunicata). Mar. Ecol. Prog. Ser. 252, 143–157.

Miller, C.B., 2004. Biological Oceanography. Blackwell Publishing, Malden, USA.

Ohman, M.D., 2012. Estimation of mortality for stage-structured zooplankton populations: what is to be done? J. Mar. Syst. 93, 4–10.

Ohman, M.D., Eiane, K., Durbin, E.G., Runge, J.A., Hirche, H.-J., 2004. A comparative study of Calanus finmarchicus mortality patterns at five localities in the North Atlantic. ICES J. Mar. Sci. 61, 687–697.

Ohman, M.D., Hsieh, C.-H., 2008. Spatial differences in mortality of Calanus pacificus within the California Current System. J. Plankton Res. 30, 359–366.

Ohman, M.D., Powell, J.R., Picheral, M., Jensen, D.W., 2012. Mesozooplankton an particulate matter responses to a deep-water frontal system in the southern California Current System. J. Plankton Res. 34, 815–827.

Pesant, S., Legendre, L., Gosselin, M., Ashjian, C., Booth, B., Daly, K., Fortier, L., Hirche, H.-J., Michaud, J., Smith, R.E.H., Smith, S., Smith Jr., W.O., 1998. Pathways of carbon cycling in the euphotic zone: the fate of large-sized phytoplankton in the Northeast Water Polynya. J. Plankton Res. 20, 1267–1291.

Platt, T., Denman, K., 1978. The structure of pelagic marine ecosystems. Rapp. P.-V. Réun. Cons. Int. Explor. Mer 173, 60–65.

Ploug, H., Iversen, M., Fischer, G., 2008. Ballast, sinking velocity, and apparent diffusivity within marine snow and zooplankton fecal pellets: implication for substrate turnover by attached bacteria. Limnol. Oceanogr. 53, 1878–1886.

Plourde, S., Maps, F., Joly, P., 2009. Mortality and survival in early stages control recruitment in Calanus finmarchicus. J. Plankton Res. 31, 371–388.

Poulet, S.A., Ianora, A., Laabir, M., Klein Breteler, W.C.M., 1995. Towards the measurement of secondary production and recruitment in copepods. ICES J. Mar. Sci. 52, 359–368.

Reigstad, M., Carrol, J., Slagstad, D., Ellingsen, I., Wassmann, P., 2011. Intra-regional comparison of productivity, carbon flux and ecosystem composition within the northern Barents Sea. Prog. Oceanogr. 90, 33–46.

Reigstad, M., Wexels Riser, C., Wassmann, P., Ratkova, T., 2008. Vertical export of particulate organic carbon: attenuation, composition and loss rates in the northern Barents Sea. Deep-Sea Res. II 55, 2308–2319.

Riemann, L., Nielsen, T.G., Kragh, T., Richardson, K., Parner, H., Jakobsen, H.H., Munk, P., 2011. Distribution and production of plankton communities in the subtropical convergence zone of the Sargasso Sea. I. Phytoplankton and bacterioplankton. Mar. Ecol. Prog. Ser. 426, 57–70.

Runge, J.A., Roff, J.C., 2000. The measurement of growth and reproductive rates. In: Harris, R.P., Wiebe, P.H., Lenz, J., Skjoldal, H.R., Huntley, M. (Eds.), ICES Zooplankton Methodology Manual. Academic Press, London, UK, pp. 401–454.

Rutledge, G.K., Alpert, J., Ebuisaki, W., 2006. NOMADS: a climate and weather model archive at the national oceanic and atmospheric administration. Bull. Am. Meteorol. Soc. 87, 327–341.

Sato, 2003. Species-specific house productivity of appendicularians. Mar. Ecol. Prog. Ser. 259, 163–172.

Schultes, S., Lopes, R.M., 2009. Laser Optical Plankton counter and Zooscan intercomparison in tropical and subtropical marine ecosystems. Limnol. Oceanogr. Methods 7, 771–784.

Sheldon, R.W., Prakash, A., Sutcliffe, W.H.J., 1972. The size distribution of particles in the ocean. J. Limnol. Oceanogr. 17, 327–340.

Silvert, W., Platt, T., 1978. Energy flux in the pelagic ecosystem: a time-dependent equation. Limnol. Oceanogr. 23, 813–816.

Skarðhamar, J., Reigstad, M., Carroll, J., Eiane, K., Riser, C.W., Slagstad, D., 2011. Effects of mortality changes on biomass and production in Calanus spp. populations. Mar. Ecol. Prog. Ser. 12, 129–145.

Slagstad, D., Tande, K.S., 1990. Growth and production dynamics of Calanus glacialis in an arctic pelagic food web. Mar. Ecol. Prog. Ser. 63, 189–199.

Søreide, J.E., Hop, H., Falk-Petersen, S., Gulliksen, B., Hansen, E., 2003. Macrozooplankton communities and environmental variables in the Barents Sea marginal ice zone in late winter and spring. Mar. Ecol. Prog. Ser. 263, 43–64.

Stenevik, E.K., Melle, W., Gaard, E., Gislason, A., Broms, C.T.A., Prokopchuk, I., Ellertsen, B., 2007. Egg production of Calanus finmarchicus — A basin-scale study. Deep-Sea Res. II 54, 2672–2685.

Stige, L., Lajus, D.L., Chan, K.-S., Dalpadado, P., Basedow, S., Berchenko, I., Stenseth, N.C., 2009. Climatic forcing of zooplankton dynamics is stronger during low densities of planktivorous fish. Limnol. Oceanogr. 54, 1025–1036.

Tande, K.S., 1989. Calanus in North Norwegian fjords and in the Barents Sea. Polar Res. 10, 389–407.

Tarling, G.A., Stowasser, G., Ward, P., Poulton, A.J., Zhou, M., Venables, H.J., McGill, R.A.R., Murphy, E.J., 2012. Seasonal trophic structure of the Scotia Sea pelagic ecosystem considered through biomass spectra and stable isotope analysis. Deep-Sea Res. II 59–60, 222–236.

Turner, J.T., 2004. The importance of small planktonic copepods and their roles in pelagic marine food webs. Zool. Stud. 43, 1021–5506.

Våge, S., Basedow, S.L., Tande, K.S., Zhou, M., 2014. Physical structure of the Barents Sea Polar Front near Storbanken in August 2007. J. Mar. Syst 130, 256–262 (this volume).

Vidal, J., 1980. Physio-ecology of zooplankton. 4. Effects of phytoplankton concentration, temperature, and body size on the net production efficiency of Calanus pacificus. Mar. Biol. 56, 203–211.

Yebra, L., Hernández-León, S., 2004. Aminoacyl-tRNA synthetases activity as a growth index in zooplankton. J. Plankton Res. 351–356.

Zhou, M., 2006. What determines the slope of a plankton biomass spectrum? J. Plankton Res. 28 (5), 437–448.

Zhou, M., Carlotti, F., Zhu, Y., 2010. A size-spectrum zooplankton closure model for ecosystem modelling. J. Plankton Res. 32, 1147–1165.

Zhou, M., Huntley, M., 1997. Population dynamics theory of plankton based on biomass spectra. Mar. Ecol. Prog. Ser. 159, 61–73.

Zhou, M., Tande, K.S., Zhu, Y., Basedow, S., 2009. Productivity, trophic levels and size spectra of zooplankton in northern Norwegian shelf regions. Deep-Sea Res. II. http://dx.doi.org/10.1016/j.dsr2.2008.11.018.